

Study of hysteresis and chaotic dynamics in bulk ferromagnet

Pek-Lan Toh and Siew-Choo Lim

School of Physics, Universiti Sains Malaysia, 11800 USM, Pulau Pinang.

(Received 30 June 2009)

In this paper, we studied phenomenologically and numerically the ferromagnetic phase transition and dynamic responses of bulk ferromagnet. We used Landau free energy density expansion and applied the calculus of variations to formulate the second order ferromagnetic phase transition. Then these are combined with Landau-Lifshitz (LL) equation of motion in the study of chaotic dynamics of the bulk ferromagnet. The results are presented graphically by using several different applied fields and frequencies.

I. INTRODUCTION

Since the beginning of the nineteenth century, ferromagnets have induced strong theoretical interests due to high application potentials. These important applications are magnetic recording process, cores for electromagnets, electric motors, transformers, generators and etc. [1]. In 1976, Sukiennick used the phenomenological Ginzburg-Landau (GL) theory, which was combined with the scaling theory to review the magnetic phase transition in thin films [2]. Besides this, phenomenological study on ferromagnetic systems based on thermodynamic considerations was proposed by Jiles and Atherton in 1983 [3]. Arai *et al.* had reported the use of Yttrium Iron Garnet (YIG) as a thin film inductor and the range of frequency was examined up to 1 GHz for the first time in 1991. The sandwich type of YIG exhibited an inductance by forty times larger than a similar air core inductor [4]. In theoretical studies, Borisov *et al.* have discovered the chaotic motion of the magnetization in the ferromagnetic resonance region with various applied fields by using Landau-Lifshitz (LL) equation of motion [5]. In 2001, Garcia-Cervera and Weinan have compared the hysteresis loops from those effective dynamics simulations with LL equation of motion [6]. Recently, Liu and Garcia-Cervera have studied the effects of incorporating thermal noise into LL equation of motion for the ferromagnetic thin films. They have reported the relation between the thermal noise and switching fields in the hysteresis loop [7]. From the literature survey it seems that the researches on chaotic dynamics are still left behind. So, it is of interest to carry out a more significant study of the chaotic dynamics in ferromagnetic system.

In this paper, we carry out a phenomenological study of hysteresis and chaotic dynamics in ferromagnetic system. In this approach, we consider the system in its ferromagnetic phase can be represented solely by the Landau free energy density expansion in terms of its order parameter, i.e. \mathbf{M} , its material constants and temperature. This means we have neglecting the microscopic effects, i.e. domain wall movements in the presence of applied field, and all the quantum mechanical interactions that usually considered

in the research of ferromagnetic system. In these contexts, we have applied the calculus of variation on Landau free energy density expansion of the ferromagnetic system in order to formulate the second order ferromagnetic phase transition. The variations of Landau free energy density expansion are combined with LL equation of motion for the studies of dynamics in the ferromagnetic system. The results are solved numerically and presented graphically by using material constants of YIG in the presence of applied fields with various amplitudes and frequencies. Because of the frequencies of the applied field are much lower than the ferromagnetic resonance frequency, typically in the microwave region, the responses from the numerical simulations can be considered as quasi-dynamic, or quasi static.

II. THEORETICAL MODELLING

IIa. Formalism

We begin with Landau free energy density expansion of the ferromagnetic system:

$$F = F_0 + \frac{1}{2}\alpha_2\mathbf{M}^2 + \frac{1}{4}\alpha_4\mathbf{M}^4 + \dots - \mathbf{B} \cdot \mathbf{M} \quad (1)$$

where F_0 is the free energy density other than the contribution of order parameter in ferromagnetic phase. α_2 , α_4 are Landau coefficients, \mathbf{M} is magnetization, and \mathbf{B} is applied field. In Eq. (1), the second order term in the right hand side is temperature dependent, and this is shown in its Landau coefficient:

$$\alpha_2 = \frac{\alpha_0(T - T_C)}{M_S^2} \quad (2)$$

where $\alpha_0 = \frac{C_{ex}}{(T_C - T)a^2}$, T is the temperature, T_C , C_{ex} ,

M_S and a are ferromagnetic material parameters with

respect to Curie temperature, exchange constant, saturation magnetization and lattice constant. The free energy density expansion in Eq. (1) is truncated at the fourth order term, which is relevant to ferromagnetic system with second order phase transition [2,8,9]. In equilibrium, the variation of free energy is a minimum, i.e.

$$\frac{\delta F}{\delta M_i} = 0. \quad (3)$$

If the system is oriented such that $\mathbf{M} = M_z \hat{k}$. This yield a relation of the Landau coefficients

$$\alpha_4 = -\frac{\alpha_2}{M_S^2} \quad (4)$$

and the equation of state:

$$\alpha_2 M_z + \alpha_4 M_z^3 - B_z = 0. \quad (5)$$

The graph of equation of state is shown in Fig. 1.

Fig. 1 shows the saturation magnetization, M_S , and coercive magnetic field, B_C for a few temperatures. Clearly, M_S and B_C are increased as temperature is decreased. In the following calculations, we adopt M_S at $T = 300$ K.

Iib. Dynamics Responses of Bulk Ferromagnet

To study the dynamic responses of bulk ferromagnet with respect to applied field, $\mathbf{B}(t)$, we considered the magnetization, \mathbf{M} as 3-dimensional vector with Cartesian components $\mathbf{M} = M_x \hat{i} + M_y \hat{j} + M_z \hat{k}$, where $|\mathbf{M}| = M_S = 1.39 \times 10^5$ A/m at $T = 300$ K [10]. In this case, the Landau free energy density expansion with $\mathbf{B}(t)$ can be written in the following form:

$$F = F_0 + \frac{1}{2} \alpha_2 [M_x^2 + M_y^2 + M_z^2] + \frac{1}{4} \alpha_4 [M_x^2 + M_y^2 + M_z^2]^2 - B_z(t) M_z. \quad (6)$$

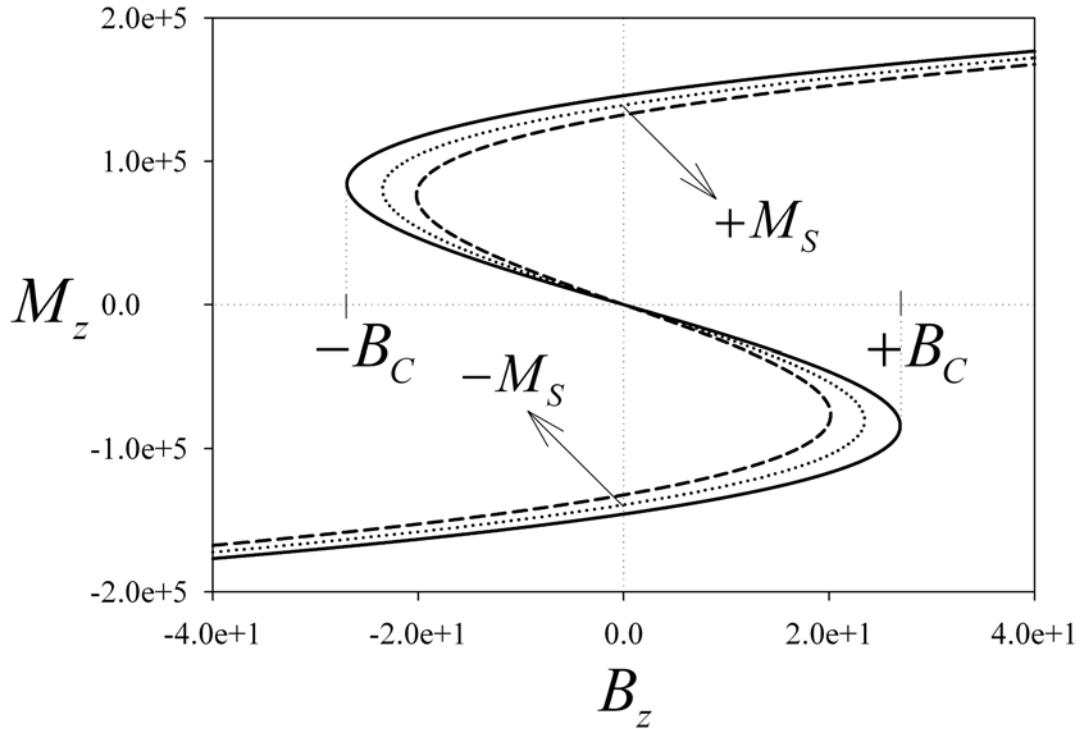


FIG. 1. M_z versus B_z for bulk YIG with $T = 275$ K (solid line), 300 K (dotted line), and 325 K (dash line).

The dynamic responses of the magnetization are described by the phenomenological LL equation of motion:

$$\frac{d\mathbf{M}}{dt} = -\gamma\mathbf{M} \times \mathbf{B}_{eff} - \Gamma\mathbf{M} \times [\mathbf{M} \times \mathbf{B}_{eff}] \quad (7)$$

where $\gamma = \frac{ge}{2m_e}$ is the gyromagnetic ratio, $\Gamma = \frac{\gamma\eta}{M_s}$ is the Gilbert-damping constant, $g \approx 2$ is the Lande g -factor for ferromagnetic system, e is the magnitude of the electron charge, m_e is the electron mass and $\eta \approx 0.01 - 0.1$ is the dimensionless damping coefficient [6,7,10,11]. $\mathbf{B}_{eff} = \mu_0\mathbf{H}_{eff}$ is the effective field derived from the variation of the free energy density in Eq. (1), i.e.

$$\mathbf{B}_{eff,i} = -\frac{\delta F}{\delta M_i}. \quad (8)$$

Evaluation of Eq. (8) resulting the explicit relations of the effective field to the variation of the free energy density with respect to the ferromagnetic order parameter M_i :

$$\mathbf{B}_{eff,i} = -\left\{ \frac{d}{dt} \left[\frac{\partial F}{\partial \dot{M}_i} \right] - \frac{\partial F}{\partial M_i} \right\}. \quad (9)$$

Since the free energy density do not contain \dot{M}_i , the first term on the right of the Eq. (9) is zero. The effective field is simplified to

$$\mathbf{B}_{eff,i} = \frac{\partial F}{\partial M_i}. \quad (10)$$

In component form, this is:

$$\mathbf{B}_{eff} = \frac{\partial F}{\partial M_x} \hat{i} + \frac{\partial F}{\partial M_y} \hat{j} + \frac{\partial F}{\partial M_z} \hat{k} \quad (11)$$

where

$$\begin{aligned} \frac{\partial F}{\partial M_x} &= \alpha_2 M_x + \alpha_4 M_x [M_x^2 + M_y^2 + M_z^2] \\ \frac{\partial F}{\partial M_y} &= \alpha_2 M_y + \alpha_4 M_y [M_x^2 + M_y^2 + M_z^2] \\ \frac{\partial F}{\partial M_z} &= \alpha_2 M_z + \alpha_4 M_z [M_x^2 + M_y^2 + M_z^2] - B_z(t). \end{aligned} \quad (12)$$

Substitution of Eqs. (11) and (12) into Eq. (7) yield

$$\begin{aligned} \frac{d\mathbf{M}}{dt} &= B_z(t)[\gamma M_y + \Gamma M_x M_z] \hat{i} + B_z(t)[\Gamma M_y M_z - \gamma M_x] \hat{j} \\ &\quad - B_z(t)\Gamma[M_x^2 + M_y^2] \hat{k}. \end{aligned} \quad (13)$$

The three Cartesian components at the right hand side of Eq. (13) are independent of each others. This yields three coupled first order differential equations, which can be solved only numerically.

III. NUMERICAL RESULTS AND DISCUSSION

In this study, we used the material parameter of YIG for the numerical simulations of Eq. (13). These are $a = 12.376 \text{ \AA}$, $C_{ex} = 1.3 \times 10^{-11} \text{ J/m}$, $M_s = 1.39 \times 10^5 \text{ A/m}$, $\gamma = 1.76 \times 10^{11} \text{ T}^{-1}\text{s}^{-1}$, $T_C = 560 \text{ K}$ [2,4,5,9], and the damping constant is assumed $\eta = 0.01$. The initial values of magnetization are assumed as

$$\begin{aligned} M_x &= M_s \sin \theta \cos \phi \\ M_y &= M_s \sin \theta \sin \phi \\ M_z &= M_s \cos \theta \end{aligned} \quad (14)$$

with $\theta = 30^\circ$ and $\phi = 30^\circ$. We adopt the fourth-order Runge-Kutta method for the numerical simulations of the dynamics of magnetization with respect to applied field, $B_z(t) = B_0 \cos(\omega t)$. B_0 is the amplitude of the time dependent magnetic field and $\omega = 2\pi f$ is its angular frequency. In order to see frequency effects, we chose $f = 25 \text{ Hertz}$, 50 Hertz , and 100 Hertz in the numerical simulations. The studies of magnetization dynamic behaviours are based on the numerical curves of M_i versus t , M_i versus $B_z(t)$, and $\frac{dM_i}{dt}$ versus M_i , where $i = x, y, \text{ and } z$.

IIIa. Quasi-Periodic Response

The numerical graphs for different values of B_0 are shown in Figs. 2 to 5. Fig. 2 shows a full cycle of time dependent applied field for $f = 25 \text{ Hertz}$, with amplitude $B_0 = 1.0 \times 10^{-20} \text{ Tesla}$. This amplitude is changed for the observation of its influence on the dynamics in ferromagnetic system. The numerical simulations showed that there is no change in M_x , M_y and M_z for $B_0 \leq 3.0 \times 10^{-18} \text{ Tesla}$, because of the applied field is too weak. This is followed by gradually increase the value of B_0 . The graphs with significant effects of B_0 are shown in Figs. 3 to 5. For $B_0 \leq 5.0 \times 10^{-10} \text{ Tesla}$, the period of the dynamic responses of M_z are the same as

input frequencies. These are shown in Fig. 3(a) for three different input frequencies. The corresponding phasor diagrams are shown in Figs. 3(b) and 3(c). The dynamic behaviours of M_x and M_y are similar to M_z , with differences in magnitude only. This means that the amplitude of this applied field is still too weak to excite any nonlinear behaviour. These quasi-periodic responses remain for the higher frequencies, i.e. chose $f = 50$ Hertz and 100 Hertz. However, the amplitudes of M_i decrease when the frequency increases. This verifies that for higher frequencies, the system has shorter time to fully response to the applied field. These are shown in Fig. 3(a), with $M_z(t)_{f=25\text{Hz}} > M_z(t)_{f=50\text{Hz}} > M_z(t)_{f=100\text{Hz}}$. The corresponding phasor diagrams in Figs. 3(b) and 3(c) showed the same features, with the size of the loops decrease with increasing frequencies.

IIIb. Chaotic Responses

The onset of chaotic responses or non-periodicity are observed only in M_x and M_y components for $B_0 > 5.0 \times 10^{-10}$ Tesla. The quasi-periodic response remains in M_z component. For $B_0 = 1.0 \times 10^{-8}$ Tesla, the periods of dynamic responses in M_x are being eight-folded for $f = 25$ Hertz, five-folded for $f = 50$ Hertz, and three-folded for $f = 100$ Hertz. These are shown in Fig. 4(a). The corresponding phasor diagrams are shown in Figs. 4(b) and 4(c). These responses are chaotic because of their phasor diagrams are never repeating and overlapping. The dynamic responses of M_y are similar to M_x . Further numerical simulations showed that when B_0 is increased, the chaotic responses are getting more intense. These chaotic responses of M_x and M_y can be observed only for $B_0 < 3.31543 \times 10^{-7}$ Tesla for $f = 25$ Hertz, $B_0 < 3.3403 \times 10^{-7}$ Tesla for $f = 50$ Hertz, and $B_0 < 3.3928 \times 10^{-7}$ Tesla for $f = 100$ Hertz.

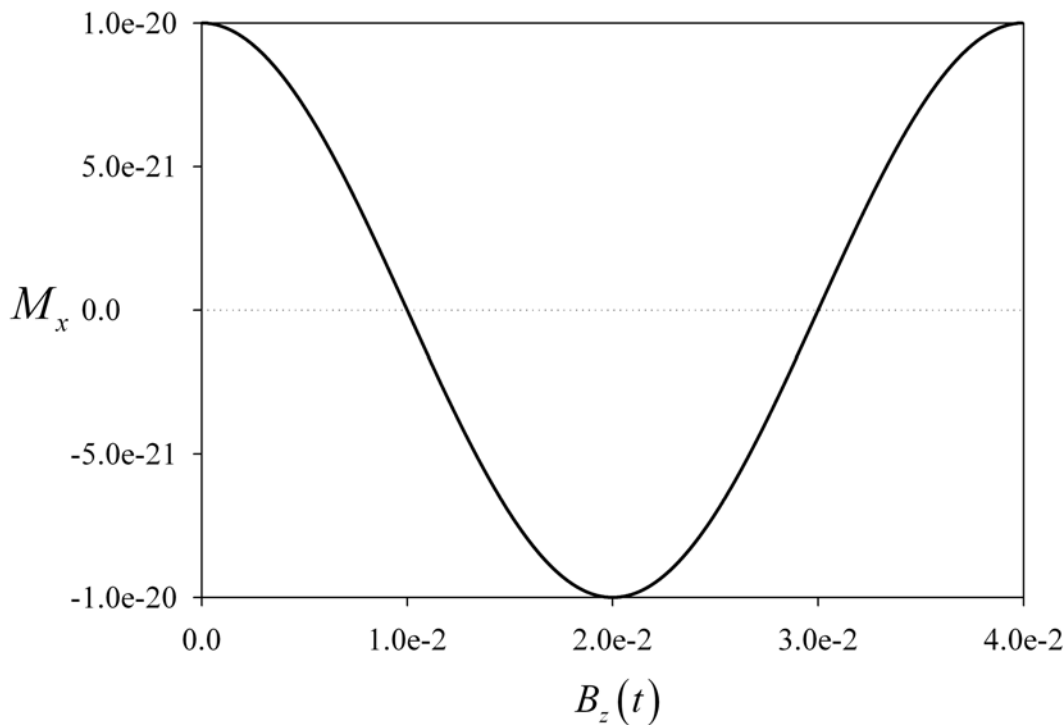


FIG. 2. A full cycle of $B_z(t) = B_0 \cos(\omega t)$ versus t . The amplitude is $B_0 = 1.0 \times 10^{-20}$ Tesla.

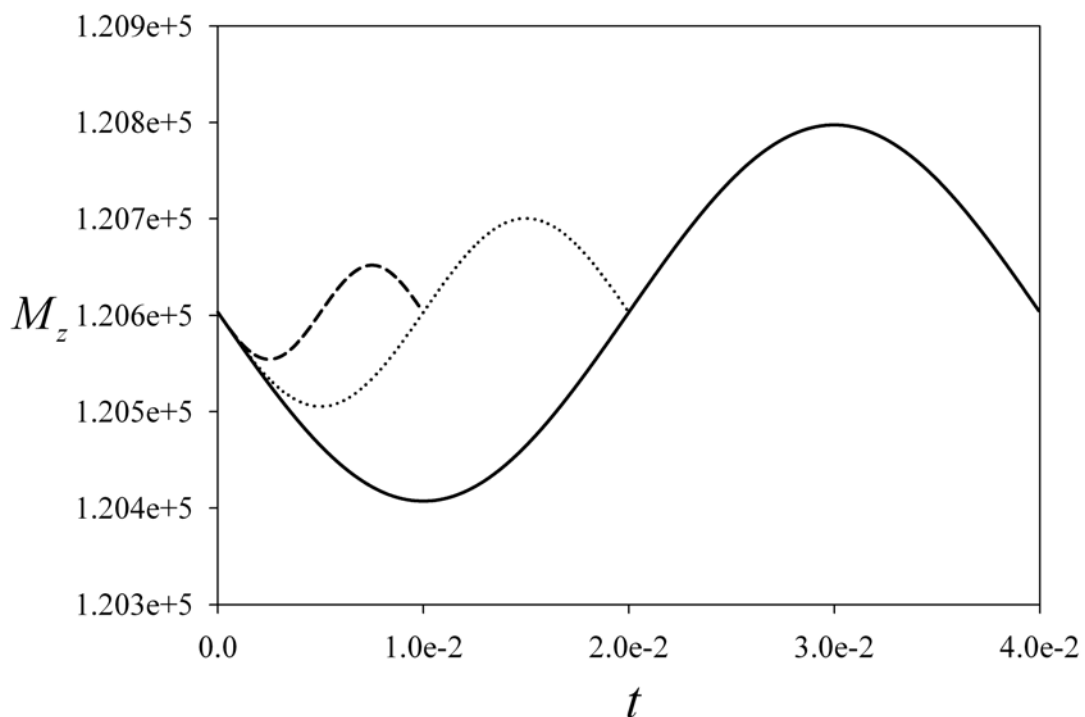


FIG. 3(a). M_z versus t for $f=25$ Hertz (solid line), 50 Hertz (dotted line), and 100 Hertz (dash line) with $B_0 = 5.0 \times 10^{-10}$ Tesla.

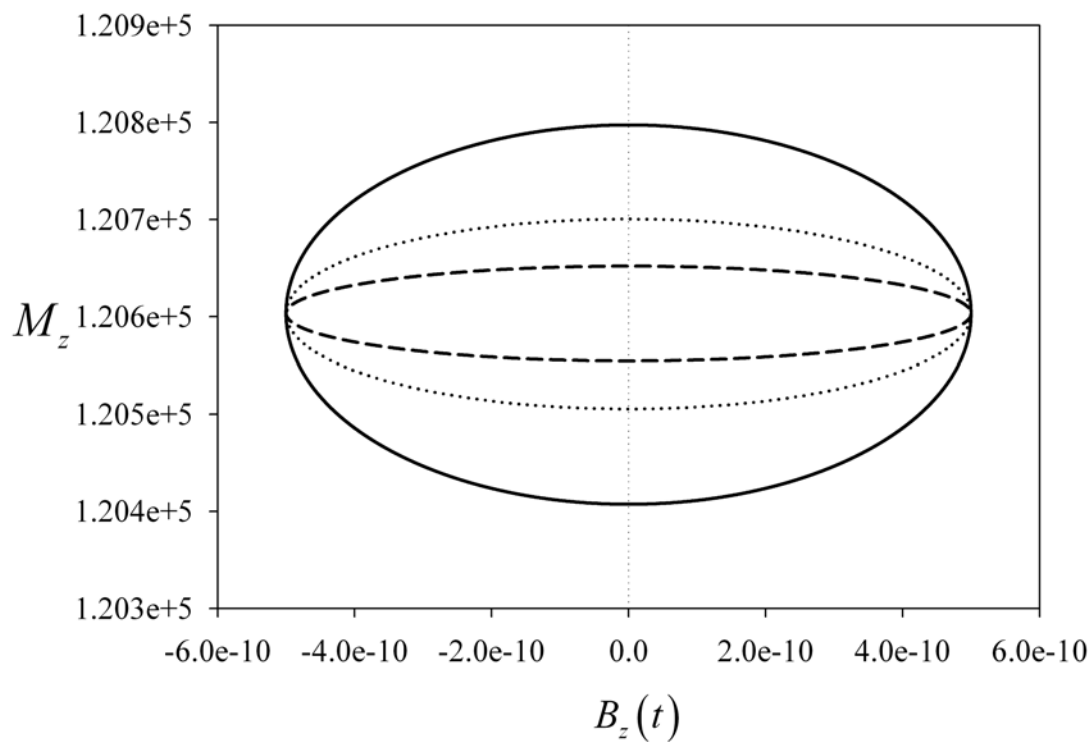


FIG. 3(b). M_z versus $B_z(t)$ for $f=25$ Hertz (solid line), 50 Hertz (dotted line), and 100 Hertz (dash line) with $B_0 = 5.0 \times 10^{-10}$ Tesla.

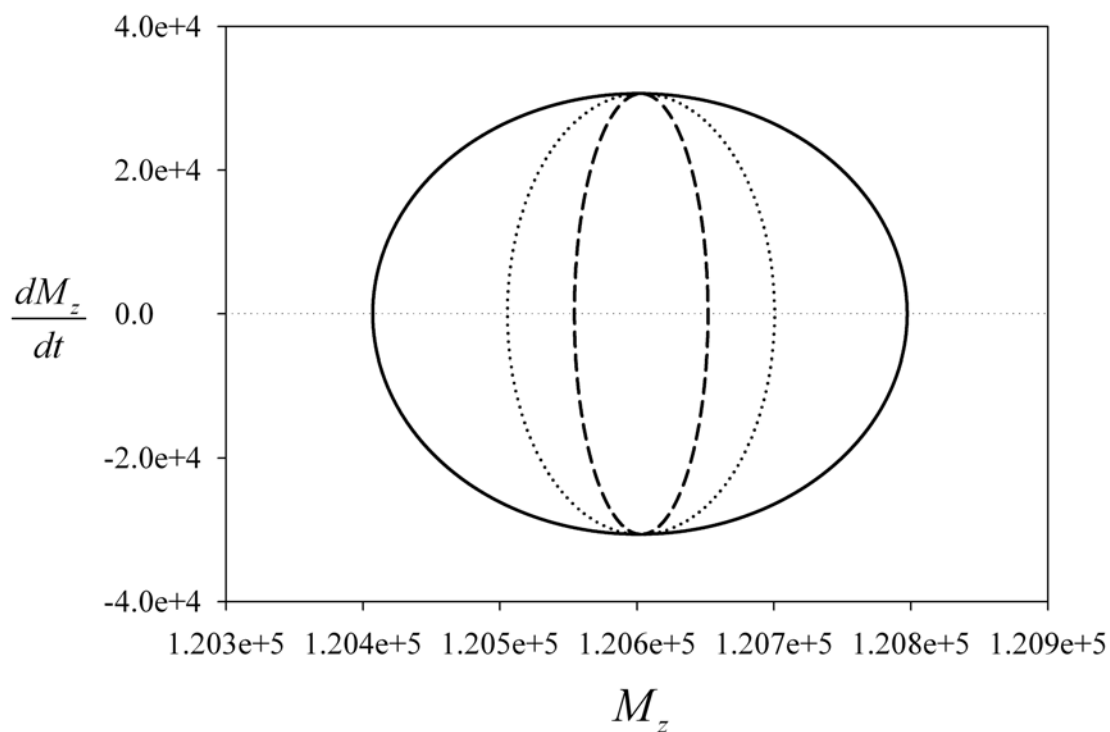


FIG. 3(c). $\frac{dM_z}{dt}$ versus M_z for $f=25$ Hertz (solid line), 50 Hertz (dotted line), and 100 Hertz (dash line) with $B_0 = 5.0 \times 10^{-10}$ Tesla.

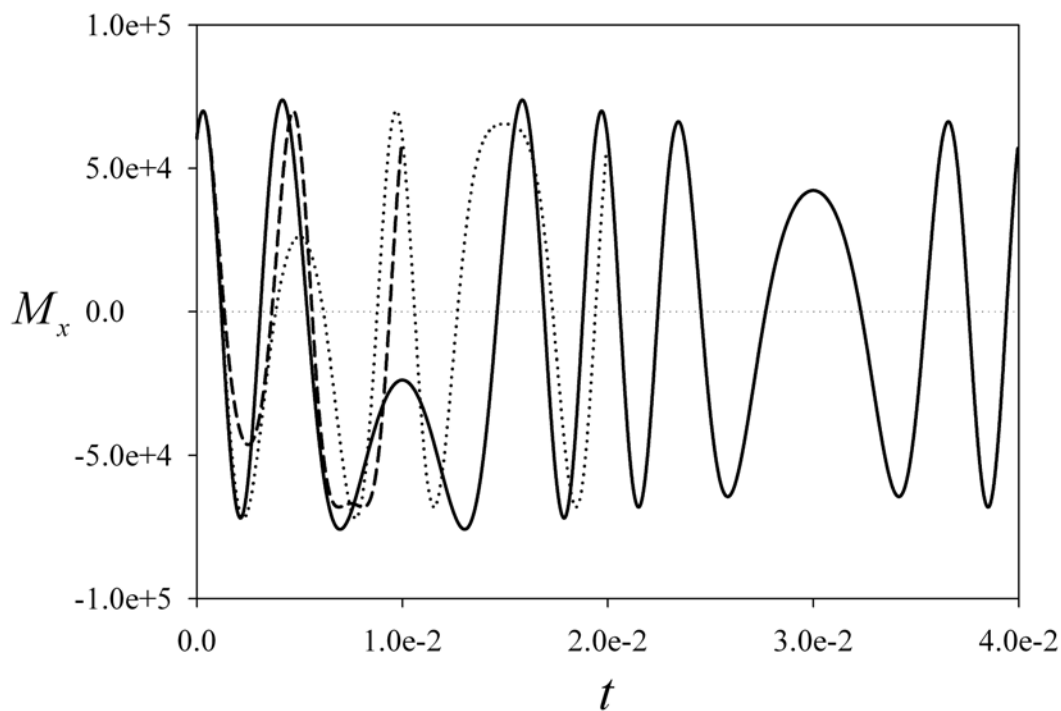


FIG. 4(a). M_x versus t for $f=25$ Hertz (solid line), 50 Hertz (dotted line), and 100 Hertz (dash line) with $B_0 = 1.0 \times 10^{-8}$ Tesla.

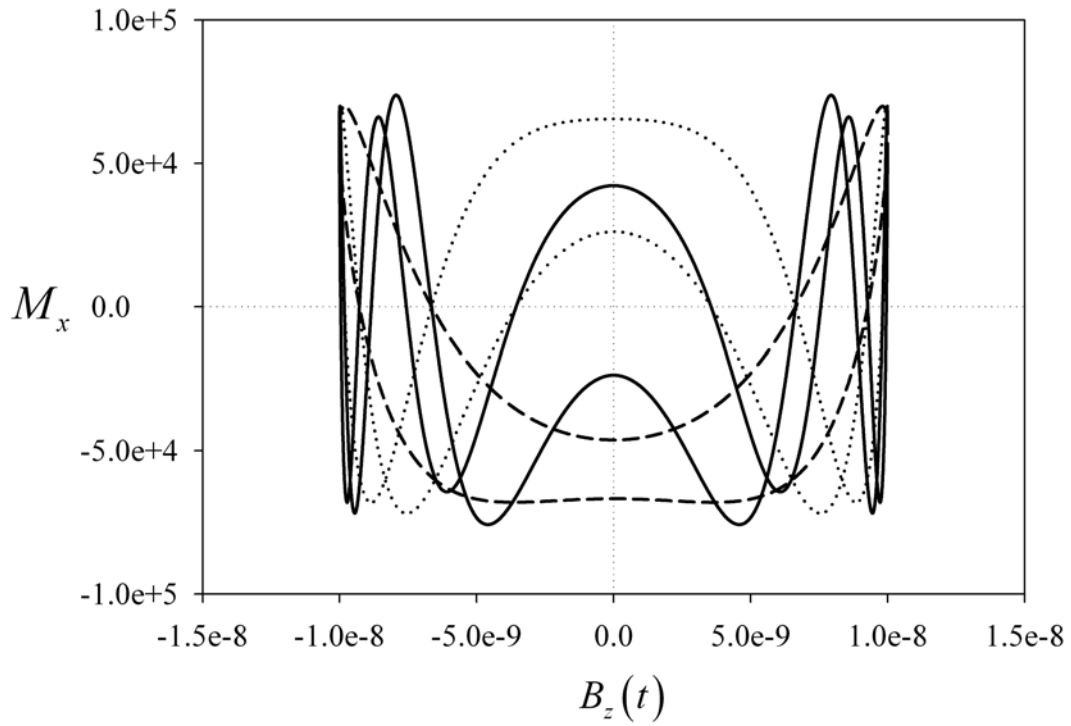


FIG. 4(b). M_x versus $B_z(t)$ for $f = 25$ Hertz (solid line), 50 Hertz (dotted line), and 100 Hertz (dash line) with $B_0 = 1.0 \times 10^{-8}$ Tesla.

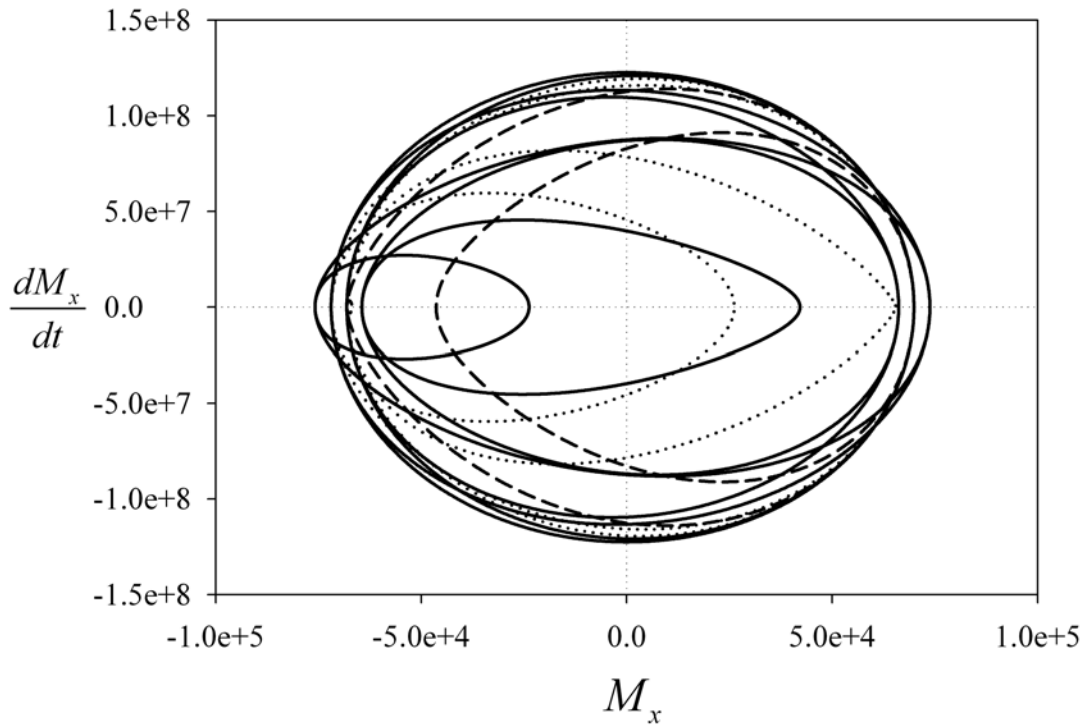


FIG. 4(c). $\frac{dM_x}{dt}$ versus M_x for $f = 25$ Hertz (solid line), 50 Hertz (dotted line), and 100 Hertz (dash line) with $B_0 = 1.0 \times 10^{-8}$ Tesla.

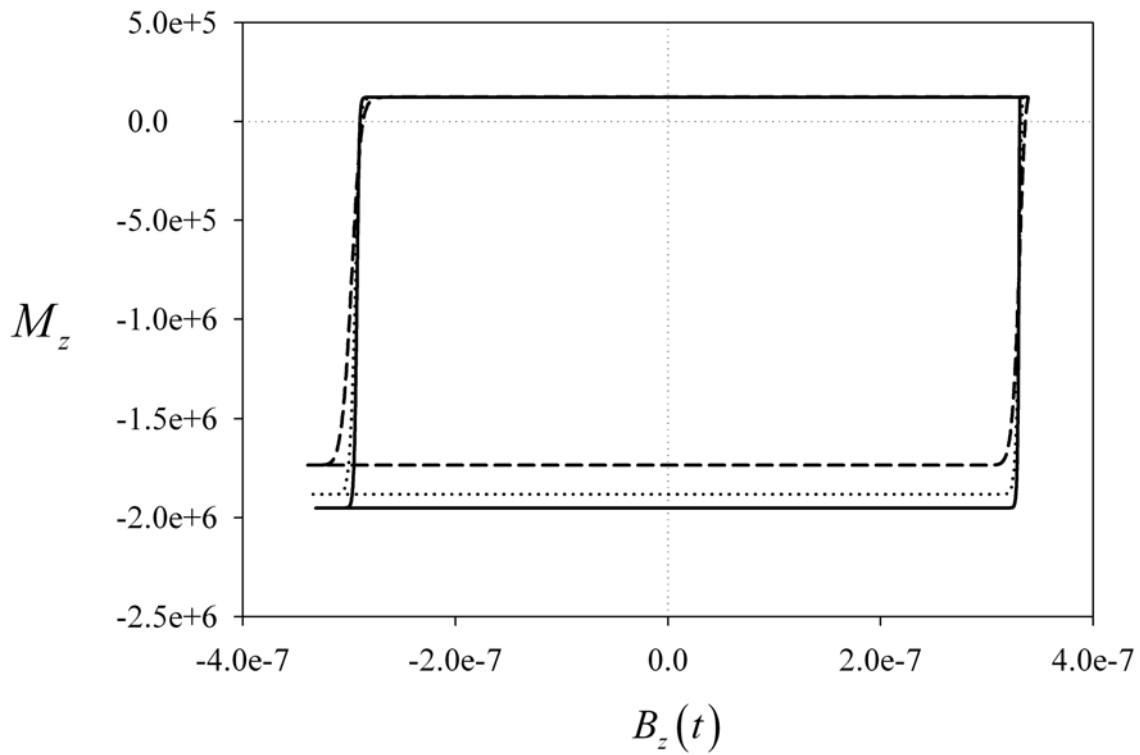


FIG. 5. M_z versus $B_z(t)$ for $f = 25$ Hertz with $B_0 = 3.31354 \times 10^{-7}$ Tesla (solid line), for $f = 25$ Hertz with $B_0 = 3.33805 \times 10^{-7}$ Tesla (dotted line), and for $f = 25$ Hertz with $B_0 = 3.38982 \times 10^{-7}$ Tesla (dash line).

IIIc. Dynamic Responses of M_z

For $B_0 > 8.0 \times 10^{-8}$ Tesla, the quasi-periodic responses in M_z disappear. However, the range of B_0 for M_z to show nonlinear responses is different if compare with M_x and M_y components. When $B_0 \geq 3.21 \times 10^{-7}$ Tesla, the hysteresis effects become obvious. For $f = 25$ Hertz, the reversal of M_z occurs, the hysteresis loops can be observed for 3.3135×10^{-7} Tesla $\leq B_0 < 3.31543 \times 10^{-7}$ Tesla. For $f = 50$ Hertz, the hysteresis loops can be observed for 3.338×10^{-7} Tesla $\leq B_0 < 3.3403 \times 10^{-7}$ Tesla, and for $f = 100$ Hertz, the hysteresis loops can be observed for 3.3897×10^{-7} Tesla $\leq B_0 < 3.3928 \times 10^{-7}$ Tesla. Complete hysteresis loop for three different frequencies are shown in Fig. 5 with $B_0 = 3.31354 \times 10^{-7}$ Tesla for $f = 25$ Hertz, $B_0 = 3.33805 \times 10^{-7}$ Tesla for $f = 50$ Hertz, and $B_0 = 3.38982 \times 10^{-7}$ Tesla for $f = 100$ Hertz.

IV. CONCLUSION

The main focus of this study is the formulation of dynamic equations of the magnetization vector of the ferromagnetic system by combining the Landau-Lifshitz equation of motion and variation of Landau free energy density expansion of the magnetization. The resulting equations of motion of the magnetization vector are three coupled first order nonlinear differential equations, which are corresponding to the three Cartesian components of the magnetization vector. These coupled nonlinear differential equations can be solved only numerically.

By using the forth-order Runge-Kutta method, the observation of chaotic responses in magnetization is determined by proper selection of initial conditions of M_i . The simulated results show distinctive effects of the amplitudes and frequencies of the applied field to the dynamic responses of the magnetizations. For M_z component, the analysis shows that the occurrences of hysteresis curve depend on the amplitudes and frequencies of the applied field, i.e. for $f = 25$ Hertz, 50 Hertz, and 100 Hertz, the hysteresis effects can be observed for B_0 within the range 3.3135×10^{-7} Tesla – 3.31542×10^{-7} Tesla, 3.338×10^{-7} Tesla – 3.3402×10^{-7}

Tesla, and 3.3897×10^{-7} Tesla – 3.3927×10^{-7} Tesla correspondingly.

The quasi-periodic response of all magnetization components can be observed with $B_0 \leq 5.0 \times 10^{-10}$ Tesla for $f = 25$ Hertz, $B_0 \leq 1.0 \times 10^{-9}$ Tesla for $f = 50$ Hertz, and $B_0 \leq 2.1 \times 10^{-9}$ Tesla for $f = 100$ Hertz, whereas the bifurcations of the periods or non-periodicity responses of the x - and y - components of magnetization can be observed for B_0 within the range 5.1×10^{-10} Tesla – 3.31542×10^{-7} Tesla for $f = 25$ Hertz, 1.1×10^{-9} Tesla – 3.3402×10^{-7} Tesla for $f = 50$ Hertz, and 2.2×10^{-9} Tesla – 3.3927×10^{-7} Tesla for $f = 100$ Hertz.

From the numerical simulations, the results show that with the presence of low frequencies and low amplitudes of applied fields, which can be generated easily in laboratory, can excite various nonlinear responses in the ferromagnetic systems, e.g. multiple-folded of input frequencies or period bifurcations, chaotic behaviours of the magnetizations, and hysteresis effects, which are strongly initial conditions dependent. We conclude that the Landau phenomenological model and classical approaches, i.e. Landau free energy expansion, calculus of variations, and LL torque equation of motion, exhibit the intrinsic rich nonlinear and chaotic phenomena in the ferromagnetic system.

ACKNOWLEDGEMENTS

This study was supported by Usm Fellowship, Institute of Postgraduate Studies, Universiti Sains Malaysia and FRGS Grant, Ministry of Higher Education, Malaysia.

REFERENCES

- [1] R. Gerber, C. D. Wright and G. Asti, *Applied Magnetism*, Klumer Academic Publishers, Netherlands (1994).
- [2] A. Sukiennicki, IEEE Transactions on Magnetism, **MAG-12(12)**, 90 (1976).
- [3] D. C. Jiles and D. L. Atherton, IEEE Transactions on Magnetism, **MAG-19**, 2183 (1983).
- [4] K. I. Arai, M. Yamaguchi, H. Ohzeki and M. Matsumoto, IEEE Transactions on Magnetism, **27(6)**, 5337 (1991).
- [5] A. B. Borisov, B. N. Filippov, V. V. Zverev and B. Y. Rubinstein, Journal of Magnetism and Magnetic Materials, **110**, 202 (1992).
- [6] C. Garcia-Cervera and E. Weinan, Journal of Applied Physics, **90(1)**, 370 (2001).
- [7] D. Liu and C. Garcia-Cervera, Journal of Applied Physics, **98**, 023903 (2005).
- [8] T. R. Kirkpatrick and D. Belitz, Physics Review B, **67**, 024419 (2003).
- [9] M. I. Kaganov and A. N. Omel' Yanchuk, Soviet Physics JETP, **34(4)**, 895 (1972).
- [10] S. C. Lim, Ph. D Thesis, University Sains Malaysia (1999).
- [11] E. Weinan, W. Q. Ren and E. Vanden-Eijnden, Journal of Applied Physics, **93(14)**, 023903 (2003).

